# A computationally compact representation of Magnetic-Apex and Quasi-Dipole coordinates with smooth base vectors

J. T. Emmert,[1] A. D. Richmond,[2] and D. P. Drob[1]

Received 1 February 2010; revised 26 March 2010; accepted 6 April 2010; published 28 August 2010.

[1] Many structural and dynamical features of the ionized and neutral upper atmosphere are strongly organized by the geomagnetic field, and several magnetic coordinate systems have been developed to exploit this organization. Quasi-Dipole coordinates are appropriate for calculations involving horizontally stratified phenomena like height-integrated currents, electron densities, and thermospheric winds; Modified Apex coordinates are appropriate for calculations involving electric fields and magnetic field-aligned currents. The calculation of these coordinates requires computationally expensive tracing of magnetic field lines to their apexes. Interpolation on a precomputed grid provides faster coordinate conversions, but requires the overhead of a sufficiently fine grid, as well as finite differencing to obtain coordinate base vectors. In this paper, we develop a compact and robust representation of the transformation from geodetic to Quasi-Dipole (QD), Apex, and Modified Apex coordinates, by fitting the QD coordinates to spherical harmonics in geodetic longitude and latitude. With this representation, base vectors may be calculated directly from the expansion coefficients. For an expansion truncated at order 6, the fitted coordinates deviate from the actual coordinates by a maximum of 0.4°, and typically by 0.1°. The largest errors occur in the equatorial Atlantic region. Compared to interpolation on a pre-computed grid, the spherical harmonic representation is much more compact and produces smooth base vectors. An algorithm for efficiently and concurrently computing scalar and vector spherical harmonic functions is provided in the appendix. Computer code for producing the expansion coefficients and evaluating the fitted coordinates and base vectors is included in the auxiliary material.

**Citation:** Emmert, J. T., A. D. Richmond, and D. P. Drob (2010), A computationally compact representation of Magnetic-Apex and Quasi-Dipole coordinates with smooth base vectors, *J. Geophys. Res.*, *115*, A08322, doi:10.1029/2010JA015326.

## 1. Introduction

[2] Many structural and dynamical features of the ionized and neutral upper atmosphere are strongly organized by the geomagnetic field, and several magnetic coordinate systems have been developed to exploit this organization. The simplest are centered dipole coordinates, which consist of a simple rotation of geocentric coordinates (geocentric coordinates originate at the center of the Earth, with the z axis toward the north rotational pole [*Vallado*, 2001]). Centered dipole colatitude ($\pi/2 - \lambda_d$, where $\lambda_d$ is centered dipole latitude) is measured from the magnetic south pole, which is located in the geocentric northern hemisphere. Centered dipole longitude, $\phi_d$, is measured eastward from the meridian (in the geocentric western hemisphere) that connects the geocentric and centered dipole poles.

[3] Eccentric dipole coordinates additionally include a translation of the origin of the magnetic coordinate system. *Fraser-Smith* [1987] reviewed centered and eccentric dipole coordinates and described how to compute their transformation parameters from the Gauss coefficients of the International Geomagnetic Reference Field (IGRF).

[4] *Hultqvist* [1958a, 1958b] computed parameterized departures of geomagnetic field lines from a pure dipole, for 36 discrete longitudes at 10° intervals. These computations were used in the development of Corrected Geomagnetic (CGM) coordinates [*Mayaud*, 1960; *Hakura*, 1965; *Gustafsson et al.*, 1992]. CGM coordinates are computed by tracing a field line from the point of interest up to its intersection with the dipole equator, and then back down along the dipole field line to the original geocentric radius. The dipole latitude and longitude of that point constitute the CGM coordinates of the original point. At low latitudes, there are regions where the field line never intersects the dipole equatorial plane, and interpolation is used to compute CGM coordinates in these regions. *Papitashvili et al.* [1992, 1997] extended the CGM approach to magnetospheric heights, taking into account field distortions produced by magnetospheric currents.

[5] The location of a field line's apex is the basis of three magnetic coordinate systems: Magnetic Apex [*VanZandt*

[1]Space Science Division, U.S. Naval Research Laboratory, Washington, DC, USA.
[2]High Altitude Observatory, National Center for Atmospheric Research, Boulder, Colorado, USA.


0148-0227/10/2010JA015326

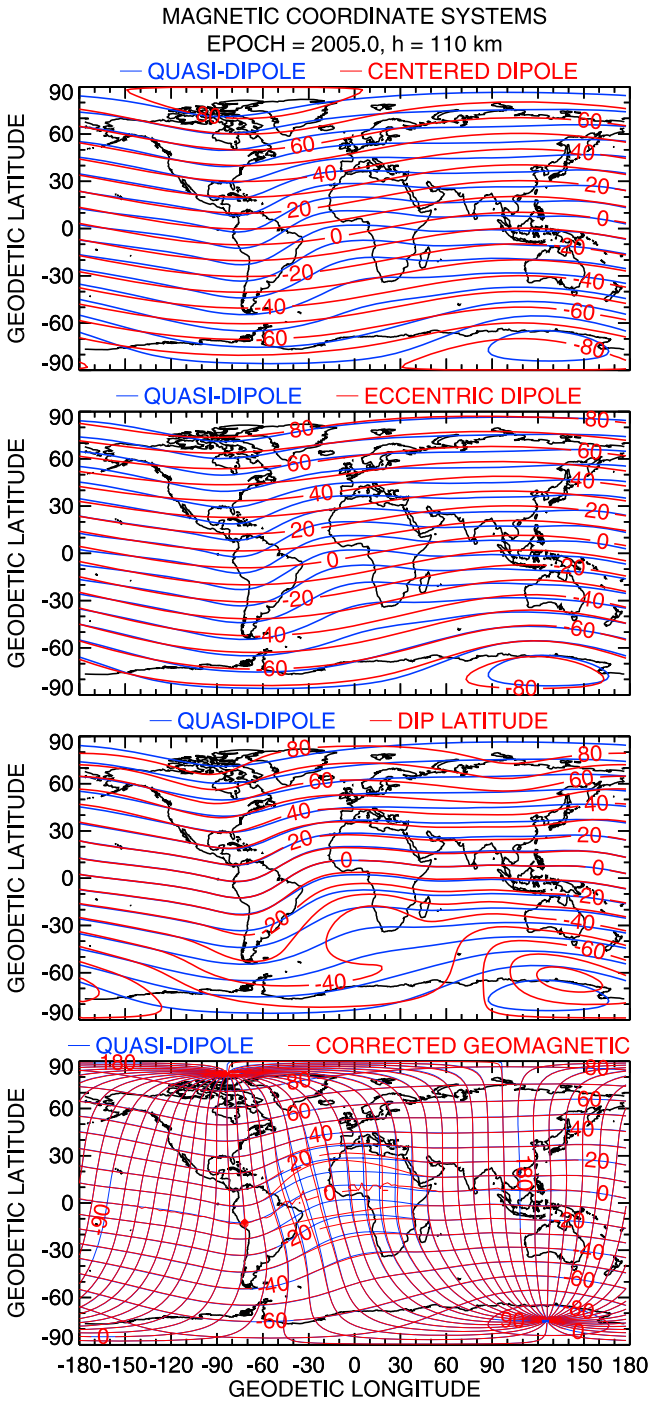


**Figure 1.** Comparison of Quasi-Dipole coordinates (blue) with other magnetic coordinate systems (red) at epoch 2005.0 and height 110 km.

*et al.*, 1972], Modified Apex [*Richmond*, 1995], and Quasi-Dipole [*Richmond*, 1995] coordinates. Their definition is motivated by the field line equation for a dipole field: If the geomagnetic field were exactly dipolar, then the radius $r$ of a field line would be

$$r = r_0 \cos^2 \lambda_d \tag{1}$$

at centered dipole latitude $\lambda_d$, where $r_0$ is the apex radius.

[6] Apex longitude, $\phi_A$, is defined as the centered dipole longitude of the apex location. Apex latitude is defined by

$$\lambda_A \equiv \pm \cos^{-1}\left(\frac{R_{eq}}{R_{eq}+h_A}\right)^{1/2} \tag{2}$$

where $h_A$ is the geodetic height of the apex above the reference ellipsoid, $R_{eq}$ = 6378.137 km is the equatorial radius of the ellipsoid [*National Imagery and Mapping Agency* (*NIMA*), 2000], and $\cos^{-1}$ denotes the arccosine function. The sign of Apex latitude is determined by the sign of the vertical component of the magnetic field. Modified Apex coordinates use a slightly different definition for latitude, but the longitude is the same:

$$\begin{aligned} \lambda_m &\equiv \pm \cos^{-1}\left(\frac{R_E+h_R}{R_E+h_A}\right)^{1/2} \\ \phi_m &\equiv \phi_A \end{aligned} \tag{3}$$

where $R_E$ = 6371.009 km is the mean radius of Earth [*NIMA*, 2000] and $h_R$ is a specified constant reference height. Except for the change in latitude sign at the magnetic equator, Apex and Modified Apex coordinates are constant along a geomagnetic field line. In contrast, Quasi-Dipole (QD) coordinates vary along a field line, but are only weakly dependent on height. QD coordinates are given by

$$\begin{aligned} \lambda_q &\equiv \pm \cos^{-1}\left(\frac{R_E+h}{R_E+h_A}\right)^{1/2} \\ \phi_q &\equiv \phi_A \end{aligned} \tag{4}$$

where $h$ is geodetic height, the third QD coordinate.

[7] Finally, two latitudinal coordinates commonly used in ionospheric physics are invariant latitude [*O'Brien et al.*, 1962] and dip latitude [e.g., *Yoshida et al.*,1960]. Invariant latitude is defined by

$$\Lambda \equiv \cos^{-1}\left(\frac{1}{L}\right)^{1/2} \tag{5}$$

where $L$ is the magnetic shell parameter [*McIlwain*, 1961]. Dip latitude is defined in terms of the local magnetic field:

$$\lambda_{dip} \equiv \tan^{-1}\left(\frac{1}{2}\tan I\right) = \tan^{-1}\left(\frac{Z}{2H}\right) \tag{6}$$

where $I$ is the downward magnetic dip angle, defined by the downward ($Z$) and horizontal ($H$) components of the field. This definition is motivated by the components of a dipole field; if the geomagnetic field were exactly dipolar (and Earth exactly spherical) then $Z$ and $H$ would be given by:

$$\begin{aligned} Z &= \frac{2|M|}{r^3}\sin\lambda_d \\ H &= \left|\frac{M}{r^3}\cos\lambda_d\right| \end{aligned} \tag{7}$$

where $M$ is the dipole moment.

[8] Figure 1 shows comparisons, at a height of 110 km, between QD coordinates and some of the other coordinates described above. Centered dipole latitude follows the main

pattern of QD latitude, but does not capture the differing offsets of the north and south magnetic poles, nor the distortions seen at low latitudes. Eccentric dipole coordinates represent the differing offsets fairly well, but do not resolve the low-latitude pattern. Dip latitude is very similar to QD latitude at low latitudes (and identical along the dip equator), but is severely distorted at mid and high latitudes. CGM coordinates are very similar to QD coordinates everywhere but the low-latitude Atlantic sector, where CGM coordinates are not well defined. This similarity extends to higher altitudes (not shown); both CGM and QD coordinates relax to centered dipole coordinates with increasing height.

[9] Except for eccentric dipole coordinates, all the coordinates systems mentioned above can be viewed as "geocentric," so it is worth pausing here to consider nomenclature. Following *Vallado* [2001], "geocentric" herein refers to the coordinate system defined by the reference ellipsoid, with the positive z axis along the northern semiminor axis and the $x$ axis pointing to the reference meridian (0° longitude). "Geocentric latitude, longitude, and radius" refer to the spherical polar form of geocentric coordinates. "Geodetic latitude" is the angle between the equatorial plane and the normal to the surface of the ellipsoid, and "geodetic height" or "height" is the distance, along this normal, between the surface and the point of interest. "Geodetic longitude" is the same as geocentric longitude. "Magnetic coordinates" collectively refers to coordinate systems based on the geomagnetic field.

[10] The calculation of apex-based and CGM coordinates consists of tracing magnetic field lines either to their apexes or to the dipole equator. To reduce the computational expense of this operation, discrete coordinate grids are usually precomputed; magnetic coordinates at desired locations can subsequently be calculated by interpolation. This approach requires the overhead of storing large interpolation grids, and interpolation near the poles demands special treatment. Furthermore, the only existing algorithm for computing base vectors involves finite differencing on the gridded values, which gives slightly discontinuous base vectors.

[11] To provide a smooth and efficient representation of CGM coordinates, *Baker and Wing* [1989] expanded the rectangular components of CGM coordinates in terms of scalar spherical harmonics. *Hein and Bhavnani* [1996] extended that approach to higher altitudes (up to 7200 km) and improved the representation of CGM coordinates in the South Atlantic Anomaly region.

[12] In this paper we apply *Baker and Wing*'s [1989] spherical harmonic fitting method to apex-based coordinates (QD, Apex, and Modified Apex coordinates), with three significant enhancements. First, we retrieve the magnetic latitude from all three fitted rectangular coordinates, rather than just the z-coordinate; this gives more robust results near the magnetic poles. Second, we incorporate the height dependence of the coordinates into the parameterization, thereby removing the need for interpolation among gridded heights. Third, we relate the magnetic coordinate base vectors to vector spherical harmonic (VSH) functions, so that the base vectors can be computed directly from the coefficients of the spherical harmonic fit.

[13] In the next section we develop the spherical harmonic representation of QD coordinates, from which Apex and Modified Apex coordinates are readily calculated. In section 3 we describe how the QD and Modified Apex base vectors can be retrieved directly from the spherical harmonic coefficients. In section 4 we present the results of the spherical harmonic fits and assess their precision and robustness. In section 5 we describe the inverse transformation. Section 6 provides a scientific application of the technique, and section 7 summarizes our results. The appendix describes an efficient algorithm for computing the associated Legendre functions and VSH functions needed to evaluate the fitted QD coordinates and base vectors.

## 2. Spherical Harmonic Representation

[14] We chose QD coordinates, rather than other coordinate systems, for our empirical fit because QD coordinates are well defined for all locations and positive heights, and because QD latitude and longitude do not depend strongly on height. Apex coordinates and Modified Apex coordinates are easily computed from QD coordinates, as shown at the end of this section.

[15] Directly fitting QD latitude and longitude as a function of geodetic latitude and longitude is not practical, due to fact that the longitude varies rapidly near the poles. Instead, the Cartesian coordinates

$$\begin{aligned} x_q &\equiv \cos\lambda_q \cos\phi_q \\ y_q &\equiv \cos\lambda_q \sin\phi_q \\ z_q &\equiv \sin\lambda_q \end{aligned} \tag{8}$$

are a convenient choice for representing QD latitude and longitude in terms of spherical harmonics of geodetic coordinates. In equation (8), three Cartesian coordinates represent two spherical coordinates on a unit sphere. Although there is some redundancy in this choice, it removes all singularities and ambiguities, which are otherwise very awkward to manage.

[16] QD latitude and longitude vary somewhat with height, relaxing to dipole coordinates with increasing height. To represent the height dependence, we use a polynomial expansion in the following reduced height parameter:

$$\rho \equiv \frac{R_E}{R_E + h} \tag{9}$$

This parameter ranges from 1 at the surface to 0 at infinity. Of course, magnetic coordinates based on the geomagnetic main field are not very useful beyond several Earth radii. However, $\rho$ provides an expedient way to represent QD coordinates as a perturbation to centered dipole coordinates, as shown below.

[17] To represent QD coordinates in terms of geodetic coordinates, we construct the following truncated expansion:

$$\begin{aligned} x_q^{fit}(\lambda_g,\phi_g,\rho) &\equiv \sum_{l=0}^{L}\sum_{m=0}^{M}\sum_{n=m}^{N} \rho^l \tilde{P}_n^m(\theta_g)\left[a_c^{lmn}\cos m\phi_g + a_s^{lmn}\sin m\phi_g\right] \\ y_q^{fit}(\lambda_g,\phi_g,\rho) &\equiv \sum_{l=0}^{L}\sum_{m=0}^{M}\sum_{n=m}^{N} \rho^l \tilde{P}_n^m(\theta_g)\left[b_c^{lmn}\cos m\phi_g + b_s^{lmn}\sin m\phi_g\right] \\ z_q^{fit}(\lambda_g,\phi_g,\rho) &\equiv \sum_{l=0}^{L}\sum_{m=0}^{M}\sum_{n=m}^{N} \rho^l \tilde{P}_n^m(\theta_g)\left[c_c^{lmn}\cos m\phi_g + c_s^{lmn}\sin m\phi_g\right] \end{aligned} \tag{10}$$

where $\{\lambda_g, \phi_g\}$ are geodetic latitude and longitude, $\theta_g = \pi/2 - \lambda_g$, $\tilde{P}_n^m$ are the associated Legendre functions normalized as described in the appendix, $\{L, M, N\}$ are the maximum orders of the expansion, and $\{\mathbf{a}, \mathbf{b}, \mathbf{c}\}$ are the arrays of coefficients. In equation (10) and subsequent equations, we abbreviate $\tilde{P}_n^m(\cos\theta_g)$ as $\tilde{P}_n^m(\theta_g)$.

[18] The utility of this choice of expansion becomes clear when we consider the transformation from geocentric coordinates $\{\lambda_{gc}, \phi_{gc}\}$ to centered dipole coordinates $\{\lambda_d, \phi_d\}$:

$$\begin{bmatrix} \cos\lambda_d \cos\phi_d \\ \cos\lambda_d \sin\phi_d \\ \sin\lambda_d \end{bmatrix} = \begin{bmatrix} \sin\lambda_{gc}^P \cos\phi_{gc}^P & \sin\lambda_{gc}^P \sin\phi_{gc}^P & -\cos\lambda_{gc}^P \\ -\sin\phi_{gc}^P & \cos\phi_{gc}^P & 0 \\ \cos\lambda_{gc}^P \cos\phi_{gc}^P & \cos\lambda_{gc}^P \sin\phi_{gc}^P & \sin\lambda_{gc}^P \end{bmatrix} \cdot \begin{bmatrix} \cos\lambda_{gc}\cos\phi_{gc} \\ \cos\lambda_{gc}\sin\phi_{gc} \\ \sin\lambda_{gc} \end{bmatrix} = \mathbf{R} \begin{bmatrix} P_1^1(\theta_{gc})\cos\phi_{gc} \\ P_1^1(\theta_{gc})\sin\phi_{gc} \\ P_1^0(\theta_{gc}) \end{bmatrix} \quad (11)$$

Here, $\{\lambda_{gc}^P, \phi_{gc}^P\}$ are the geocentric coordinates of the north pole of the centered dipole system, which define $\mathbf{R}$, the rotation matrix that constitutes the transformation. Centered dipole coordinates (in Cartesian form) are thus both a rotation of geocentric coordinates and a linear combination of the $n = 1$ geocentric spherical harmonics. In equation (10), the $l = 0$, $n = 1$ terms have the same form as equation (11), and since $\{\lambda_q, \phi_q\} \rightarrow \{\lambda_d, \phi_d\}$ as $\rho \rightarrow 0$, we can specify the $l = 0$ coefficients as

$$a_c^{0mn},\ a_s^{0mn},\ b_c^{0mn},\ b_s^{0mn},\ c_c^{0mn},\ c_s^{0mn} = 0\ \forall\ n \neq 1$$

$$\begin{bmatrix} a_c^{011} & a_s^{011} & a_c^{001} \\ b_c^{011} & b_s^{011} & b_c^{001} \\ c_c^{011} & c_s^{011} & c_c^{001} \end{bmatrix} = \frac{2}{\sqrt{3}} \begin{bmatrix} \sin\lambda_{gc}^P \cos\phi_{gc}^P & \sin\lambda_{gc}^P \sin\phi_{gc}^P & -\cos\lambda_{gc}^P/\sqrt{2} \\ -\sin\phi_{gc}^P & \cos\phi_{gc}^P & 0 \\ \cos\lambda_{gc}^P \cos\phi_{gc}^P & \cos\lambda_{gc}^P \sin\phi_{gc}^P & \sin\lambda_{gc}^P/\sqrt{2} \end{bmatrix} \quad (12)$$

where the numerical factors account for the normalization used for $\tilde{P}_n^m$. With this specification, equation (10) extends the transformation of equation (11) to higher-order spherical harmonics, allows it to vary with height, and treats QD coordinates as a perturbation of centered dipole coordinates. With increasing height, geocentric latitude approaches geodetic latitude, $\rho \rightarrow 0$, and equation (10) approaches equation (11).

[19] From the fitted Cartesian coordinates, QD latitude and longitude may be retrieved as follows:

$$\lambda_q^{fit} \equiv \tan^{-1}\left[\frac{z_q^{fit}}{\sqrt{\left(x_q^{fit}\right)^2 + \left(y_q^{fit}\right)^2}}\right] \qquad \phi_q^{fit} \equiv \tan^{-1}\left(\frac{y_q^{fit}}{x_q^{fit}}\right) \quad (13)$$

where $\tan^{-1}$ denotes the arctangent function; in computational practice, the use of the two-argument arctangent function avoids singularities and resolves the hemispheric ambiguity of $\phi_q^{fit}$. Although the fitted QD latitude could be computed using $\lambda_q^{fit} = \sin^{-1} z_q^{fit}$ [e.g., *Baker and Wing*, 1989], we found that this introduces numerical noise near the magnetic poles, due to the difficulty of computer representation of very small differences from +1 or −1. In contrast, $\sqrt{\left(x_q^{fit}\right)^2 + \left(y_q^{fit}\right)^2}$ is zero at the poles, so small differences are better represented numerically. On the other hand, $\sqrt{\left(x_q^{fit}\right)^2 + \left(y_q^{fit}\right)^2}$ differs very little from 1 near the magnetic equator, and suffers from a hemispheric ambiguity. In effect, $x_q^{fit}$ and $y_q^{fit}$ determine the magnitude of $\lambda_q^{fit}$ near the poles, while $z_q^{fit}$ provides the sign. At the equator, $z_q^{fit}$ determines both the sign and magnitude. The use of the arctangent function thereby provides a robust global representation, as demonstrated in section 4.

[20] From the fitted QD coordinates, Apex and Modified Apex coordinates can be computed, via equations (2)–(4), using

$$h_A^{fit} \equiv \frac{R_E + h}{\cos^2\lambda_q^{fit}} - R_E \qquad \lambda_A^{fit} \equiv \pm\cos^{-1}\left(\frac{R_{eq}}{R_{eq} + h_A^{fit}}\right)^{1/2} \qquad \phi_A^{fit} \equiv \phi_q^{fit} \quad (14)$$

$$\lambda_m^{fit} \equiv \pm\cos^{-1}\left[\left(\frac{R_E + h_R}{R_E + h}\right)^{1/2}\cos\lambda_q^{fit}\right] \qquad \phi_m^{fit} \equiv \phi_q^{fit} \quad (15)$$

where the sign of the latitude coordinates is the same as that of $\lambda_q^{fit}$.

## 3. Calculation of Base Vectors

[21] In this section we derive expressions for the base vectors $\{\mathbf{d}_1, \mathbf{d}_2, \mathbf{d}_3\}$, $\{\mathbf{e}_1, \mathbf{e}_2, \mathbf{e}_3\}$, and $\{\mathbf{f}_1, \mathbf{f}_2\}$, described by *Richmond* [1995], in terms of the expansion coefficients given in equation (10). We first derive the base vectors in terms of gradients of QD latitude and longitude. The eastward and northward base vectors $\{\mathbf{f}_1, \mathbf{f}_2\}$ of QD coordinates are given by *Richmond* [1995] as

$$\mathbf{f}_1 \equiv -(R_E + h)\mathbf{k} \times \nabla\lambda_q \qquad \mathbf{f}_2 \equiv (R_E + h)\cos\lambda_q \mathbf{k} \times \nabla\phi_q \quad (16)$$

where $\mathbf{k}$ is the upward unit vector. Because QD coordinates are not a simple rotation of geocentric coordinates, $\mathbf{f}_1$ and $\mathbf{f}_2$ are in general neither orthogonal nor of unit length [*Richmond*, 1995], but they are nonetheless very useful. A divergence-free vector field retains its divergence-free character when transformed to QD coordinates if it is expressed in terms of the $\mathbf{f}_1$ and $\mathbf{f}_2$ base vectors, as in equation (7.8) of *Richmond* [1995]. A vector field with zero vertical curl retains this character if expressed in terms of $\mathbf{k} \times \mathbf{f}_1$ and $\mathbf{k} \times \mathbf{f}_2$, as in equation (7.11) of *Richmond* [1995].

Unfortunately, there is no single set of base vectors that preserves both the divergence and curl properties of the field.

[22] The base vectors $\mathbf{d}_1$ and $\mathbf{d}_2$ of Modified Apex coordinates are oriented perpendicular to the magnetic field, in the magnetic eastward and downward/equatorward directions, respectively. For equipotential geomagnetic field lines, they vary along these lines in the same manner as the electric field. The base vector $\mathbf{d}_3$ is oriented along the magnetic field. Like the QD base vectors $\{\mathbf{f}_1, \mathbf{f}_2\}$, $\{\mathbf{d}_1, \mathbf{d}_2, \mathbf{d}_3\}$ are generally neither mutually orthogonal nor of unit length. They are defined by *Richmond* [1995] as

$$\begin{aligned}\mathbf{d}_1 &\equiv (R_E + h_R)\cos\lambda_m \nabla\phi_m \\ \mathbf{d}_2 &\equiv -\cos^2\lambda_m \cos I_m \nabla h_A = -(R_E + h_R)\sin I_m \nabla\lambda_m \\ \mathbf{d}_3 &\equiv \frac{\mathbf{d}_1 \times \mathbf{d}_2}{\|\mathbf{d}_1 \times \mathbf{d}_2\|^2}\end{aligned} \tag{17}$$

where

$$\begin{aligned}\cos I_m &\equiv \cos\lambda_m (4 - 3\cos^2\lambda_m)^{-1/2} \\ \sin I_m &\equiv 2\sin\lambda_m (4 - 3\cos^2\lambda_m)^{-1/2}\end{aligned} \tag{18}$$

From equations (3) and (4), we find

$$\nabla\phi_m = \nabla\phi_q \tag{19}$$

and

$$\begin{aligned}&\cos\lambda_m = \left(\frac{R_E + h}{R_E + h_R}\right)^{-1/2}\cos\lambda_q \\ &\Rightarrow \sin\lambda_m \nabla\lambda_m = \left(\frac{R_E + h}{R_E + h_R}\right)^{-1/2}\sin\lambda_q \nabla\lambda_q + \frac{1}{2}\left(\frac{R_E + h}{R_E + h_R}\right)^{-3/2}\cos\lambda_q \frac{\nabla h}{R_E + h_R}\end{aligned} \tag{20}$$

so that

$$\begin{aligned}\mathbf{d}_1 &= \alpha^{1/2}(R_E + h_R)\cos\lambda_q \nabla\phi_q \\ \mathbf{d}_2 &= -\left[2(R_E + h_R)\sin\lambda_q \nabla\lambda_q + \alpha\cos\lambda_q \mathbf{k}\right]\left(4/\alpha - 3\cos^2\lambda_q\right)^{-1/2} \\ \mathbf{d}_3 &= \frac{\mathbf{d}_1 \times \mathbf{d}_2}{\|\mathbf{d}_1 \times \mathbf{d}_2\|^2}\end{aligned} \tag{21}$$

where $\alpha \equiv (R_E + h_R)/(R_E + h)$.

[23] Like $\mathbf{d}_1$ and $\mathbf{d}_2$, the $\mathbf{e}_1$ and $\mathbf{e}_2$ base vectors are also perpendicular to the geomagnetic field and point generally eastward and downward/equatorward, but $\mathbf{e}_1$ and $\mathbf{e}_2$ are not necessarily parallel to their respective counterparts $\mathbf{d}_1$ and $\mathbf{d}_2$, and in contrast to $\mathbf{d}_1$ and $\mathbf{d}_2$, $\mathbf{e}_1$ and $\mathbf{e}_2$ vary along equipotential geomagnetic field lines in the same manner as the $\mathbf{E} \times \mathbf{B}/B^2$ drift velocity instead of as the electric field. They and the field-aligned base vector $\mathbf{e}_3$ can be straightforwardly calculated from their defining equations [*Richmond*, 1995]:

$$\begin{aligned}\mathbf{e}_1 &\equiv \mathbf{d}_2 \times \mathbf{d}_3 \\ \mathbf{e}_2 &\equiv \mathbf{d}_3 \times \mathbf{d}_1 \\ \mathbf{e}_3 &\equiv \mathbf{d}_1 \times \mathbf{d}_2\end{aligned} \tag{22}$$

Next, using equation (8), we express the gradients of QD latitude and longitude in terms of the gradients of the corresponding Cartesian coordinates, as follows:

$$\begin{aligned}\nabla x_q &= -\cos\phi_q \sin\lambda_q \nabla\lambda_q - \sin\phi_q \cos\lambda_q \nabla\phi_q \\ \nabla y_q &= -\sin\phi_q \sin\lambda_q \nabla\lambda_q + \cos\phi_q \cos\lambda_q \nabla\phi_q \\ \nabla z_q &= \cos\lambda_q \nabla\lambda_q\end{aligned} \tag{23}$$

Manipulating to isolate $\nabla\phi_q$ and $\nabla\lambda_q$ gives

$$\begin{aligned}\cos\lambda_q \nabla\phi_q &= -\sin\phi_q \nabla x_q + \cos\phi_q \nabla y_q \\ \nabla\lambda_q &= -\left(\cos\phi_q \nabla x_q + \sin\phi_q \nabla y_q\right) z_q + \cos\lambda_q \nabla z_q\end{aligned} \tag{24}$$

Equations (16), (21), (22), and (24) thus prescribe all three sets of base vectors in terms of QD coordinates $\{\phi_q, \lambda_q\}$ and the gradients $\{\nabla x_q, \nabla y_q, \nabla z_q\}$ of their corresponding Cartesian coordinates. To evaluate the geodetic components of the gradients of the fitted QD coordinates, we first consider the gradient of a general variable $\psi$ in geodetic coordinates $\{\phi_g, \theta_g, h\}$:

$$\nabla\psi = \frac{\mathbf{e}_{\phi_g}}{r}\frac{\partial\psi}{\partial\phi_g} + \frac{\mathbf{e}_{\theta_g}}{J}\frac{\partial\psi}{\partial\theta_g} - \frac{\mathbf{k}\rho^2}{R_E}\frac{\partial\psi}{\partial\rho} \tag{25}$$

where $\mathbf{e}_{\phi_g}$, $\mathbf{e}_{\theta_g}$, and $\mathbf{k}$ are unit vectors in the eastward, southward, and upward directions, respectively; $r$ is the distance from Earth's axis; $\theta_g = \pi/2 - \lambda_g$; and $J$ is the Jacobian to transfer between $\{\theta_g, h\}$ and $\{s, r\}$ coordinates, $s$ being the northward distance from Earth's equatorial plane:

$$\begin{aligned}s &= \left[h + \frac{(1 - e^2)R_{eq}}{\left(1 - e^2\cos^2\theta_g\right)^{1/2}}\right]\cos\theta_g \\ r &= \left[h + \frac{R_{eq}}{\left(1 - e^2\cos^2\theta_g\right)^{1/2}}\right]\sin\theta_g \\ J &= \frac{\partial r}{\partial\theta_g}\cos\theta_g - \frac{\partial s}{\partial\theta_g}\sin\theta_g = h + \frac{(1 - e^2)R_{eq}}{\left(1 - e^2\cos^2\theta_g\right)^{3/2}}\end{aligned} \tag{26}$$

where $e = 0.08181919$ is the eccentricity of Earth's meridional ellipse, related to the flatness $\varepsilon = 1/298.2572$ [*NIMA*, 2000] by

$$e^2 = 2\varepsilon - \varepsilon^2 \tag{27}$$

Applying equation (25) to equation (10), we obtain the components of $\nabla x_q^{fit}$:

$$\begin{aligned}\nabla x_q^{fit} \cdot \mathbf{e}_{\phi_g} &= \frac{\sin\theta_g}{r}\sum_{l=0}^{L}\sum_{m=0}^{M}\sum_{n=m}^{N}\rho^l \tilde{W}_n^m(\theta_g)\left[-a_c^{lmn}\sin m\phi_g + a_s^{lmn}\cos m\phi_g\right] \\ \nabla x_q^{fit} \cdot \mathbf{e}_{\theta_g} &= \frac{1}{J}\sum_{l=0}^{L}\sum_{m=0}^{M}\sum_{n=m}^{N}\rho^l \tilde{V}_n^m(\theta_g)\left[a_c^{lmn}\cos m\phi_g + a_s^{lmn}\sin m\phi_g\right] \\ \nabla x_q^{fit} \cdot \mathbf{k} &= -\frac{\rho^2}{R_E}\sum_{l=1}^{L}\sum_{m=0}^{M}\sum_{n=m}^{N} l\rho^{l-1}\tilde{P}_n^m(\theta_g)\left[a_c^{lmn}\cos m\phi_g + a_s^{lmn}\sin m\phi_g\right]\end{aligned} \tag{28}$$

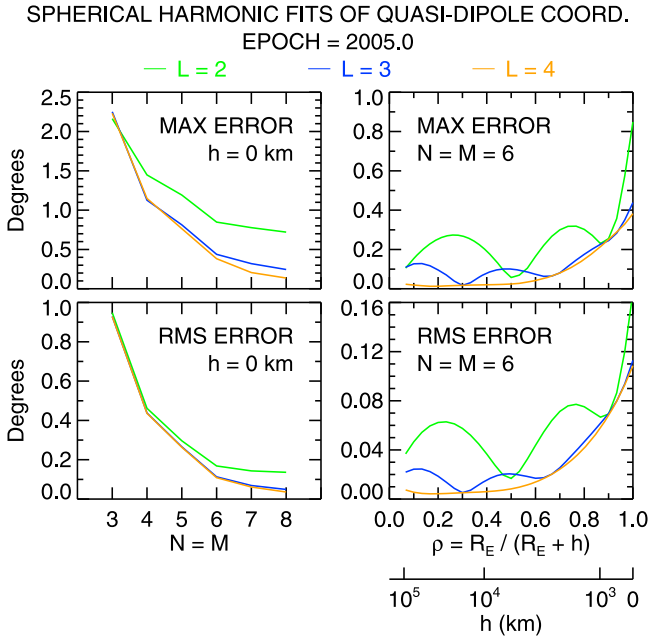


**Figure 2.** (top) Maximum and (bottom) root-mean square angular errors for spherical harmonic fits of QD coordinates at epoch 2005.0. (left) Errors at height 0 km as a function of the maximum latitudinal degree, $N$, of the expansion; the maximum longitudinal order $M$ equals $N$. (right) Errors of the $N = M = 6$ fit as a function of the reduced height parameter $\rho$. Results are shown for three different maximum vertical polynomial orders: $L = 2$ (green), $L = 3$ (blue), and $L = 4$ (orange).

where $\tilde{V}_n^m(\theta_g) \equiv \partial \tilde{P}_n^m(\theta_g)/\partial\theta_g$ and $\tilde{W}_n^m(\theta_g) \equiv m\tilde{P}_n^m(\theta_g)/\sin\,\theta_g$. The functions $\tilde{V}$ and $\tilde{W}$ are the latitude-dependent portions of VSH functions; an efficient method for computing them is given in the appendix. The expressions for the gradients of $y_q^{fit}$ and $z_q^{fit}$ are the same as equation (28), except for the labeling of the expansion coefficients. The gradients $\{\nabla x_q^{fit}, \nabla y_q^{fit}, \nabla z_q^{fit}\}$ can thereby be computed directly from the expansion coefficients.

## 4. Results

[24] We computed QD coordinates on a geodetic grid with 2° latitude spacing and 2.4° longitude spacing, and at 29 heights (evenly spaced values of $\rho$ from 1.0 to 0.067) and ten epochs (every 5 years from 1965 to 2010). We computed least squares fits of the QD coordinates using the expansions given in equation (10) and the constraints of equation (12), and weighting by cos $\lambda_g$ to compensate for the greater density of grid points with increasing latitude. We determined the expansion coefficients for the three Cartesian coordinates independently, except for the $l = 0$ coefficients, which we constrained per equation (12). Although it is possible to mutually constrain the parameters such that $(x_q^{fit})^2 + (y_q^{fit})^2 + (z_q^{fit})^2 = 1$, thereby removing the redundancy mentioned in section 2, this nonlinear constraint would be more difficult to implement, and would not be expected to significantly affect $\lambda_q^{fit}$ or $\phi_q^{fit}$.

[25] To determine an appropriate resolution for the fits, we varied the truncation orders $L$ and $N$, setting $M = N$. For each fit, we computed the maximum and root-mean square (RMS) angular separation between $\{\lambda_q, \phi_q\}$ and $\{\lambda_q^{fit}, \phi_q^{fit}\}$. The angular separation is given by:

$$\delta = \cos^{-1}\left(\sin\lambda_q \sin\lambda_q^{fit} + \cos\lambda_q \cos\lambda_q^{fit} \cos\left(\phi_q - \phi_q^{fit}\right)\right) \quad (29)$$

[26] Figure 2 (left) shows the maximum and RMS error as a function of $N$, for fits at epoch 2005.0. Results are shown at the surface ($h = 0$, $\rho = 1$), where errors are largest, for $L$ values from 2 to 4. For $L = 3$, the maximum error decreases from 2.2° to 0.3° as $N$ increases from 3 to 8. There is relatively little improvement in the fit for $N > 6$, and very little difference between the $L = 3$ and $L = 4$ fits, so henceforth we will focus on results using $\{L, M, N\} = \{3, 6, 6\}$. If a tolerance less than 0.4° is required, then higher values of $N$ can be used; values of $L$ greater than 3 are only warranted in conjunction with an increase in $N$.

[27] Figure 2 (right) shows the errors of $N = 6$ fits as a function of $\rho$. The error decreases with increasing height, as expected; above 1000 km, the maximum and RMS errors are less than half what they are at the surface.

[28] Figure 3 shows the actual and fitted QD coordinates and base vectors at 110 km and epoch 2005.0. The differences are generally imperceptible on this scale, so Figure 4 shows the angular error as a function of latitude and longitude. The largest errors (up to 0.4°) occur in the equatorial Atlantic sector; outside this region, the errors are less than 0.2°, and usually less than 0.1°. To put the Atlantic sector errors in perspective, we note that the magnetic equator in the Atlantic sector has moved northward by about 1.5° per decade over the past century [*Rangarajan*, 1994].

[29] Figure 5 shows the actual and fitted QD coordinates as a function of $\rho$, for selected geodetic latitudes along the $\phi_g = 180°$ meridian. These plots confirm that $L = 3$ provides sufficient flexibility to capture the height dependence of QD coordinates. The differences seen in the QD longitude at $\lambda_g = 0°$ and 30° are due to the horizontal resolution, not the vertical resolution.

[30] Near the QD poles, $|z_q^{fit}|$ may be greater than one, and in such regions it is not possible to retrieve $\lambda_q^{fit}$ from $z_q^{fit}$ alone. Constraining the sum of the squared Cartesian coordinates, as described at the beginning of this section, would ensure that $-1 \le z_q^{fit} \le 1$, but would not alleviate the weak variation of $z_q$ near the poles. Fortunately, the use of equation (13) to retrieve $\lambda_q^{fit}$ circumvents both problems without the need for a nonlinear constraint. This is demonstrated in Figure 6. The left panel shows fitted QD coordinates retrieved using equation (13). In the right panel, the QD latitude was retrieved using $\lambda_q^{fit} = \sin^{-1} z_q^{fit}$. The shaded area indicates the region where $z_q^{fit} > 1$ (the maximum value is 1.00055). In the right panel, this region causes the QD latitude contours to be skewed away from the pole (and undefined in the shaded region). The use of equation (13) in the left panel produces latitude contours that are centered on the pole and compatible with the fitted longitudes.

[31] Compared to interpolation on a pre-computed grid, the spherical harmonic representation of QD coordinates greatly reduces the size of the stored arrays that describe the trans-

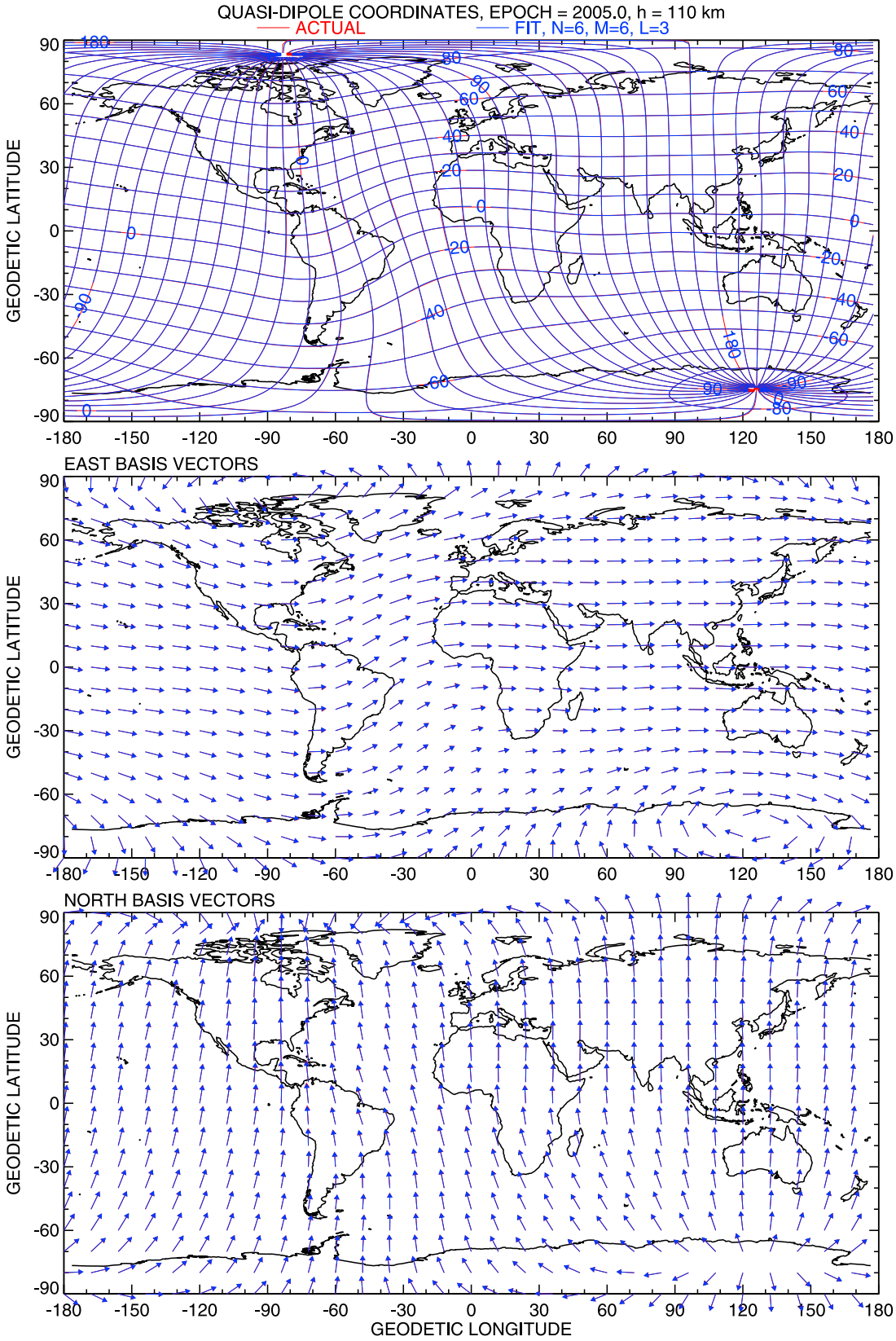


**Figure 3.** (top) Quasi-Dipole coordinates, (middle) east base vectors, and (bottom) north base vectors at height 110 km and epoch 2005.0. Actual QD values are shown in red; fitted values at a resolution of $\{L, M, N\} = \{3, 6, 6\}$ are superimposed in blue.

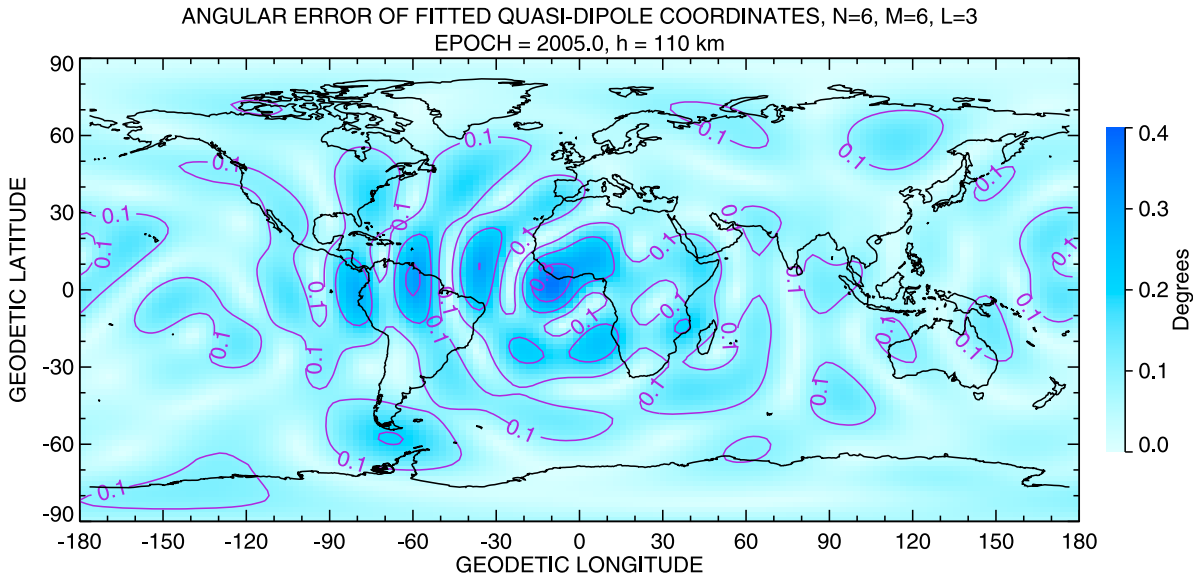


**Figure 4.** Angular difference between actual and fitted QD coordinates at height 110 km and epoch 2005.0. The fit was computed at a resolution of $\{L, M, N\} = \{3, 6, 6\}$. The contour interval is 0.1°.

formation. Using $\{L, M, N\} = \{3, 6, 6\}$ and the constraints of equation (12) requires specification of approximately 450 terms for each epoch, whereas gridded interpolation requires storage of hundreds of thousands of values. On the other hand, the spherical harmonic representation requires computation of 140 spherical harmonic and VSH functions, whereas gridded interpolation requires only a search to locate the correct cell for interpolation in addition to the interpolation itself. In speed tests, we found that the processing time required for the spherical harmonic method is only 1.5–2 times that of the interpolation method. The spherical harmonic approach thus appears to be a favorable alternative to the computational expense of the full QD calculation and to the storage overhead associated with interpolation on a pre-computed grid.

## 5. Inverse Transformation

[32] For the QD to geodetic transformation, we expanded the rectangular geodetic coordinates in terms of spherical harmonics of QD latitude and longitude. The expansion is essentially the same as equation (10), but with the $g$ and $q$ subscripts interchanged. Following *Baker and Wing* [1989] and *Hein and Bhavnani* [1996], we used the fitted QD coordinates when fitting the inverse transformation, rather than the actual QD coordinates, in order to reverse the fitted geodetic-to-QD transformation as precisely as possible. In computing the coefficients for the inverse transformation, we applied the same weights and constraints used in fitting the forward transformation.

[33] Because the expansion is truncated, the inverse transformation will not exactly recover the original geodetic coordinates (e.g., $x_g^{fit} \neq \cos\lambda_g \cos\phi_g$). At epoch 2005.0 and $h = 0$ km, with $\{L, M, N\} = \{3, 6, 6\}$, the maximum and RMS angular errors are respectively 0.81° and 0.26°. If greater precision is needed, the gradients of the coordinates can be used in conjunction with iterative computation of the forward transformation.

## 6. Scientific Application

[34] Apex-based magnetic coordinate systems are very useful for organizing upper atmospheric data and for simulations of electrodynamic phenomenon. *Richmond et al.* [2003] used QD coordinates to study the response of high-latitude neutral and ion convection patterns to changes in the interplanetary magnetic field. In the most recent version of the empirical Horizontal Wind Model, HWM07 [*Drob et al.*, 2008; *Emmert et al.*, 2008], QD coordinates are used to model geomagnetic storm effects on thermospheric winds. One shortcoming of HWM07 is that quiet time high-latitude thermospheric winds, which are similar to ion convection patterns, are not well represented by the geodetic VSH expansion used in the model. In this section we demonstrate that QD coordinates enable more reliable synthesis and interpretation of quiet time high-latitude wind data (which are generally very sparse).

[35] Figure 7 shows winds near a height of 250 km simulated by the Thermosphere Ionosphere Mesosphere Electrodynamics General Circulation Model (TIME-GCM) [*Roble and Ridley*, 1994; *Crowley et al.*, 2006]. The results are for a geomagnetically quiet day (21 June 2004, daily $Kp = 1$), and were selected from the continuous four-year simulation described by *Drob et al.* [2008]. The left-hand panels show the raw output from the model over the northern polar cap at three different universal times (UT), as a function of geodetic latitude and local solar time (LST). The wind pattern is dominated by antisunward flow over most of the region, and it includes a well-defined dusk-side convection cell.

[36] We fit the TIME-GCM winds to the spatial portion of the HWM07 formulation, which consists of VSH terms in geodetic latitude (up to degree 8), LST (up to order 3), and

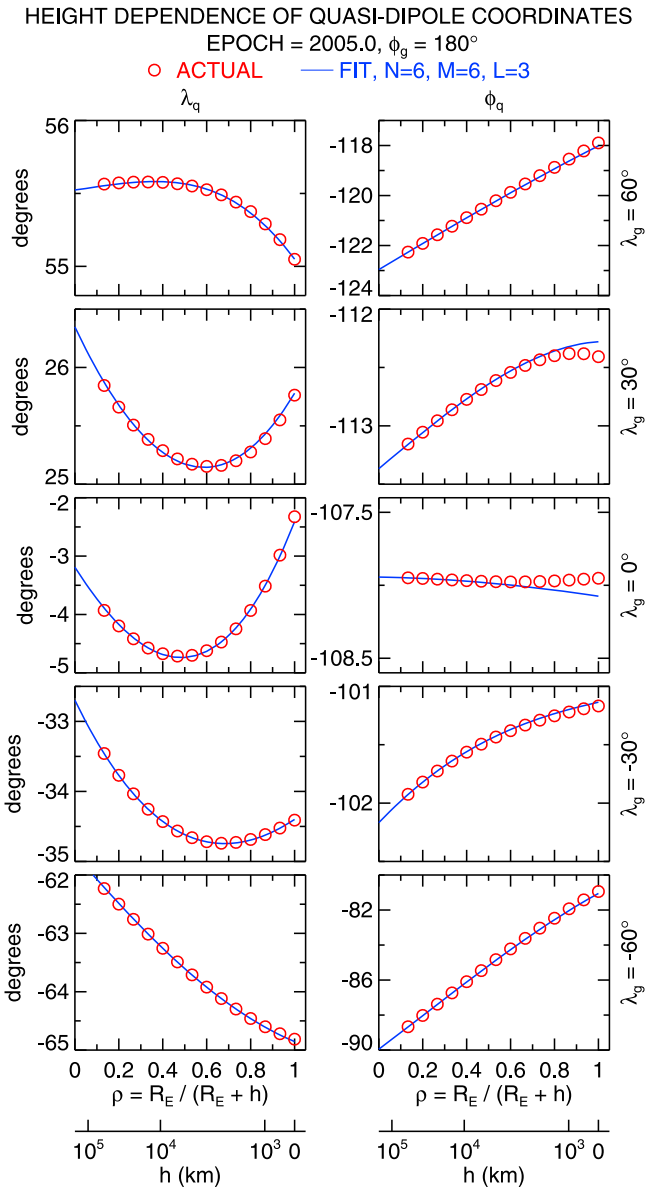


**Figure 5.** Actual (red circles) and fitted (blue line) (left) QD latitude and (right) longitude as a function the reduced height parameter $\rho$. Results are shown for epoch 2005.0, geodetic longitude 180°, and the geodetic latitudes indicated on the right of the panels.

longitude (up to order 2) [*Drob et al.*, 2008]. The middle column of plots shows the results of this fit. The fit represents the antisunward flow fairly well, but the longitude terms (which are not coupled to the local time terms) do not provide sufficient flexibility to capture the dusk convection cell.

[37] The right-hand panels show a fit of the TIME-GCM winds to VSH terms in QD latitude (up to degree 8) and QD local time (up to order 3), where QD local time is defined here as the difference between the QD longitude of a location and the QD longitude of the anti-solar point at the same height (*Richmond et al.* [2003] used the centered dipole longitude of the anti-solar point). We expressed the winds in terms of the $\mathbf{f}_1$ and $\mathbf{f}_2$ base vectors prior to computing the fit; the results in Figure 7 are shown in geodetic coordinates. This fit, which does not include explicit dependence on UT or longitude, captures the dusk cell much better than the fit to the HWM07 formulation, including the migration of the cell with UT and the cell's change of shape from 0900 UT to 1800 UT. The fit consists of 99 parameters, compared to 160 for the HWM07 formulation, but the root-mean square residual wind speed for latitudes above 60°N is considerably smaller (44 m/s versus 65 m/s). This demonstrates that the high-latitude winds are better organized in QD coordinates than in geodetic coordinates, even under geomagnetically quiet conditions. We note that TIME-GCM uses Modified Apex coordinates for representing the high-latitude electric potential that drives ion convection, so that the TIME-GCM convection pattern is organized by Modified Apex coordinates. We would therefore expect a VSH fit of the TIME-GCM winds (which are driven in part by ion convection) in QD coordinates to work better than, say, a fit in centered dipole or even eccentric dipole coordinates. Presumably, the TIME-GCM winds are realistic in this regard.

## 7. Summary

[38] We developed a parameterized representation of Quasi-Dipole (QD) latitude and longitude as a function of geodetic latitude, longitude, and height. The representation consists of an expansion of the QD rectangular coordinates in terms of geodetic spherical harmonics, with a polynomial representation of the height dependence. By retrieving the fitted QD latitude via the arctangent expression involving all three rectangular coordinates, we avoided numerical problems and ambiguities near the poles. From the fitted QD coordinates, Apex and Modified Apex coordinates are easily computed. We also derived expressions for calculating, directly from the expansion coefficients, the base vectors associated with QD and Modified Apex coordinates.

[39] Our spherical harmonic representation of apex-based coordinates provides a favorable alternative to interpolation on a pre-computed grid, which requires storage of large data arrays. It is much faster than a full computation of QD coordinates via field-line tracing. At a modest model resolution, the fitted QD coordinates typically deviate from the actual QD coordinates by 0.1°, and maximally by 0.4°.

[40] Fortran-90 code for producing the expansion coefficients and evaluating the fitted coordinates and base vectors is included in the auxiliary material.[1] Updated versions of the code will be made available through the CEDAR Data System at http://cedarweb.hao.ucar.edu/.

## Appendix A

[41] The computation of the fitted QD coordinates and base vectors requires the evaluation of both scalar and vector spherical harmonic functions. We developed an efficient algorithm for concurrently computing the three latitude-

[1] Auxiliary materials are available in the HTML. doi:10.1029/2010JA015326.

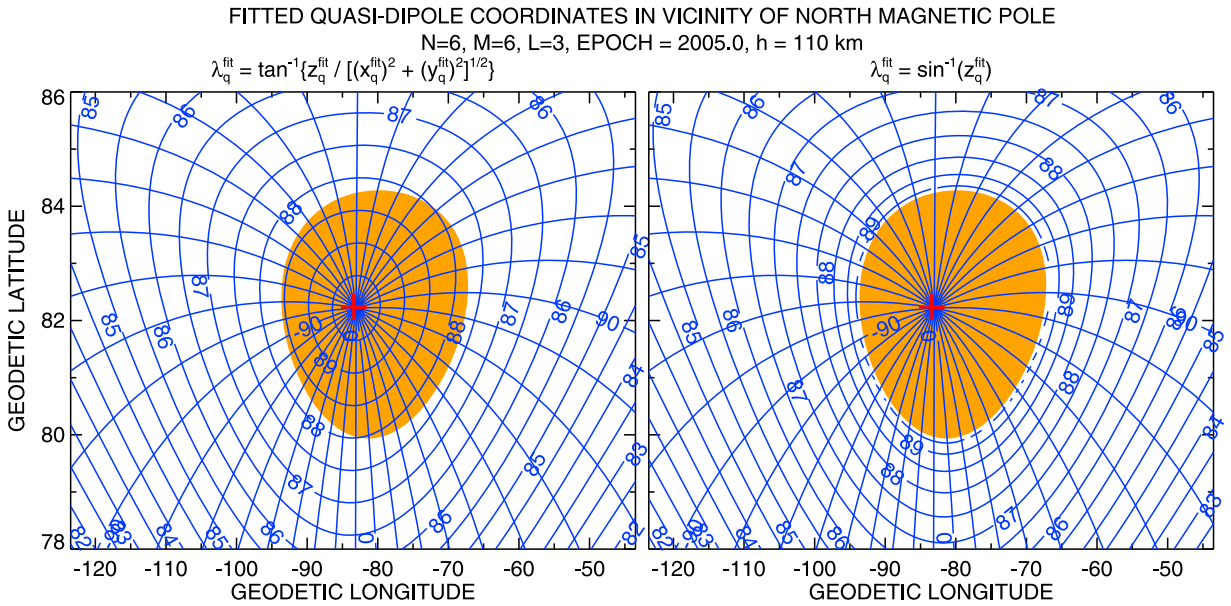


**Figure 6.** Fitted QD coordinates in the vicinity of the north magnetic pole, at height 110 km and epoch 2005.0. The fit was computed at a resolution of $\{L, M, N\} = \{3, 6, 6\}$. (left) the fitted QD latitude was retrieved using equation (13). (right) The fitted QD latitude was retrieved from $z_q^{fit}$ alone. The shaded area indicates the region where $z_q^{fit} > 1$. The red cross marks the location of the actual QD pole. The QD latitude contour interval is 0.5°, and the QD longitude contour interval is 10°.

dependent portions $P$, $V$, and $W$. We begin by defining these functions and their normalization:

$$P_n^m(\theta) \equiv \frac{1}{2^n n!}(\sin\theta)^m \frac{d^{m+n}}{dx^{m+n}}\left(x^2-1\right)^n,\ x=\cos\theta \tag{A1}$$

$$\tilde{P}_n^m(\theta) \equiv \sqrt{\frac{(2n+1)(n-m)!}{2(n+m)!}} P_n^m(\theta) \tag{A2}$$

$$\tilde{V}_n^m(\theta) \equiv \frac{d\tilde{P}_n^m(\theta)}{d\theta} \tag{A3}$$

$$\tilde{W}_n^m(\theta) \equiv \frac{m}{\sin\theta}\tilde{P}_n^m(\theta) \tag{A4}$$

where $\theta$ is colatitude, $P_n^m(\theta)$ are the unnormalized associated Legendre functions, and the normalization for $\tilde{P}_n^m(\theta)$ is the same as that used by *Swarztrauber* [1993, equation (4.20)]. The definition of $P_n^m$ in equation (A1) is commonly used in geophysics; mathematicians use a definition that differs by a factor of $(-1)^m$.

[42] We adapt the standard forward column recursion methods outlined by *Holmes and Featherstone* [2002, section 2.1]. Our strategy is to first compute

$$\tilde{\Omega}_n^m(\theta) \equiv \frac{\tilde{P}_n^m(\theta)}{\sin\theta} \tag{A5}$$

from which $\tilde{P}_n^m$ can be computed with multiplication by $\sin\theta$, $\tilde{W}_n^m$ can be computed with multiplication by $m$, and $\tilde{V}_n^m$ can be computed with the recursion relation given in equation (A8) below. The recursion relations are:

$$\tilde{\Omega}_m^m = \tilde{c}_m \tilde{P}_{m-1}^{m-1} \tag{A6}$$

$$\tilde{\Omega}_n^m = \tilde{a}_n^m \cos\theta\ \tilde{\Omega}_{n-1}^m - \tilde{b}_n^m \tilde{\Omega}_{n-2}^m \tag{A7}$$

$$\tilde{V}_n^m = n\cos\theta\ \tilde{\Omega}_n^m - \tilde{d}_n^m \tilde{\Omega}_{n-1}^m \tag{A8}$$

$$\tilde{P}_n^m = \sin\theta\ \tilde{\Omega}_n^m \tag{A9}$$

$$\tilde{W}_n^m = m\tilde{\Omega}_n^m \tag{A10}$$

$$\tilde{P}_n^0 = \tilde{a}_n^0 \cos\theta \tilde{P}_{n-1}^0 - \tilde{b}_n^0 \tilde{P}_{n-2}^0 \tag{A11}$$

$$\tilde{V}_n^0 = -\tilde{e}_n \tilde{P}_n^1 \tag{A12}$$

where

$$\tilde{a}_n^m = \sqrt{\frac{(2n-1)(2n+1)}{(n-m)(n+m)}} \tag{A13}$$

$$\tilde{b}_n^m = \sqrt{\frac{(2n+1)(n+m-1)(n-m-1)}{(n-m)(n+m)(2n-3)}} \tag{A14}$$

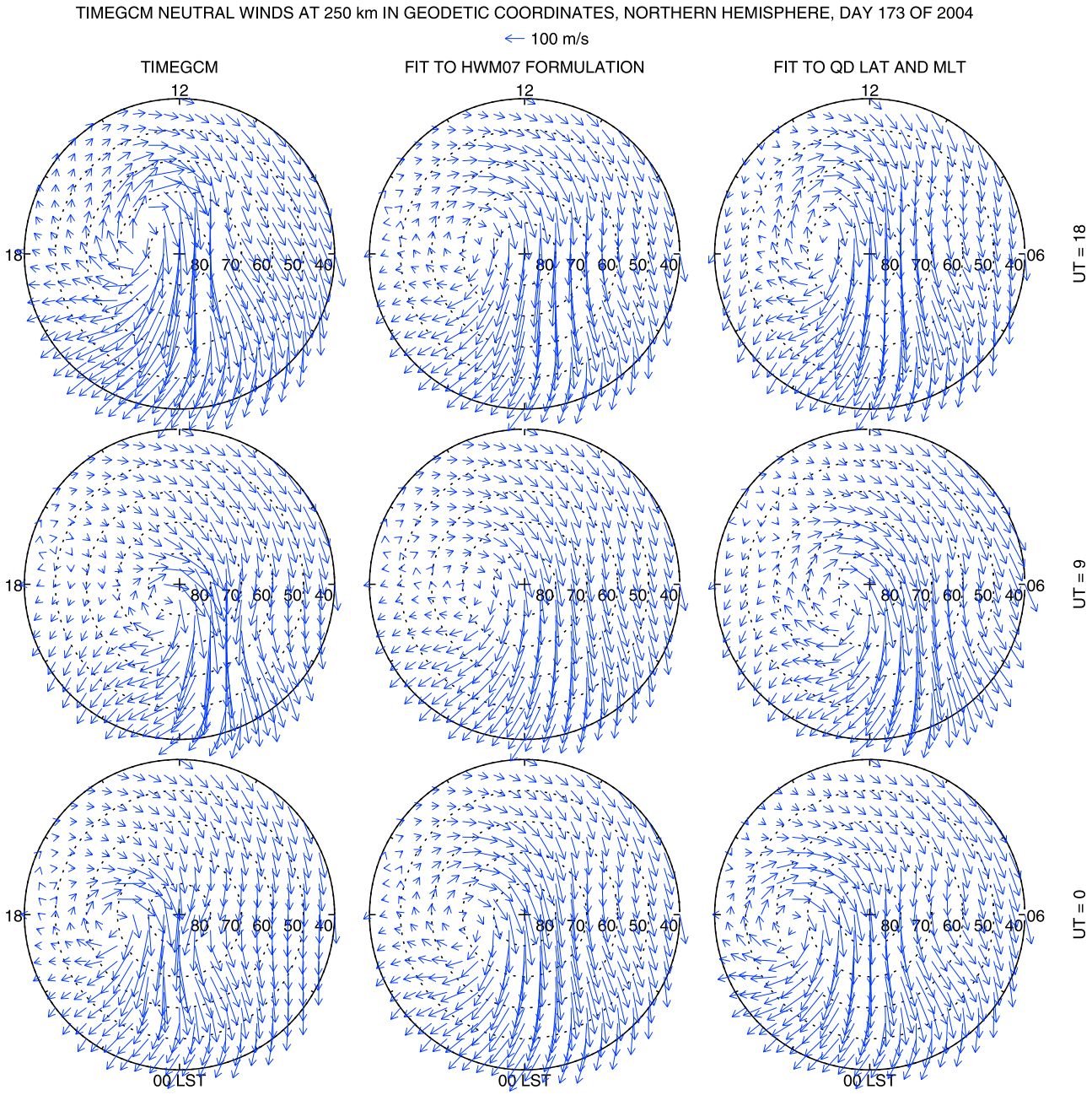


**Figure 7.** (left) TIME-GCM winds at a height of 250 km, computed for day 173 of 2004 (a geomagnetically quiet day). Winds over the Northern Hemisphere are shown as a function of geodetic latitude and local solar time, at the universal time indicated at the far right. (middle) A fit of the TIME-GCM winds to the HWM07 formulation, which consists of vector spherical harmonics in geodetic latitude (up to degree 8), local time (up to order 3), and longitude (up to order 2). (right) A vector spherical harmonic fit of the TIME-GCM winds (in terms of the $\mathbf{f}_1$ and $\mathbf{f}_2$ base vectors) as a function QD latitude (up to degree 8) and QD magnetic local time (up to order 3); results are shown in geodetic coordinates.

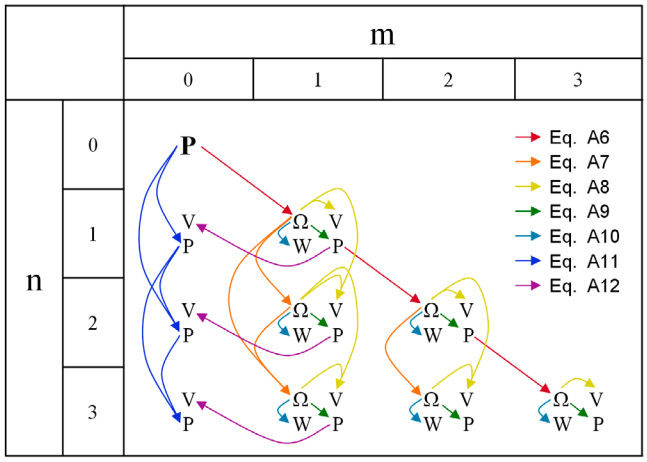


**Figure A1.** Flow diagram for computation of associated Legendre functions (P) and the latitude-dependent portion of vector spherical harmonic functions (V, W).

$$\tilde{c}_m = \sqrt{\frac{(2m+1)}{2m}} \tag{A15}$$

$$\tilde{d}_n^m = \sqrt{\frac{(n+m)(n-m)(2n+1)}{(2n-1)}} \tag{A16}$$

$$\tilde{e}_n = \sqrt{n(n+1)} \tag{A17}$$

The recursion relations given in equations (A6), (A7), (A8), and (A12) are adapted from *Holmes and Featherstone* [2002, equations (13), (11), (15), and (21)]. The recursion coefficients are largely the same as those given in *Holmes and Featherstone* [2002]; we have relabeled their $f$ as $d$, and named a new coefficient $c$. Note that the normalization for $P_n^m$ used by *Holmes and Featherstone* [2002, equation 8] is slightly different from our equation (A2), by a factor of $\sqrt{2}$ for $m = 0$ and a factor of 2 for $m > 0$.

[43] In this approach, we treat $m = 0$ separately from $m > 0$, since $\tilde{W}_n^0 = 0$ and $\tilde{\Omega}_n^0$ is undefined at the poles. Figure A1 illustrates the path of computations we use in our algorithm, starting from a single seed value of $\tilde{P}_0^0 = 1/\sqrt{2}$. The algorithm is designed to minimize the number of operations needed to populate the $P$, $V$, and $W$ matrices. After computing the recursion coefficients, a maximum of only nine multiplication and two addition operations are required to get $\tilde{P}_n^m$, $\tilde{V}_n^m$, and $\tilde{W}_n^m$ for each combination of $n$ and $m$.

[44] The normalization of $\tilde{V}_n^m$ and $\tilde{W}_n^m$ is appropriate for evaluating equation (28), which contains straightforward derivatives of the scalar spherical harmonics. However, when fitting a vector field to vector spherical harmonics, additional normalization of $\tilde{V}_n^m$ and $\tilde{W}_n^m$ is called for [e.g., *Swarztrauber*, 1993; *Killeen et al.*, 1987], so we define another set of variables with the modified normalization:

$$\overline{P}_n^m(\theta) \equiv \tilde{P}_n^m(\theta) \tag{A18}$$

$$\overline{V}_n^m(\theta) \equiv \tilde{V}_n^m(\theta) \Big/ \sqrt{n(n+1)} \tag{A19}$$

$$\overline{W}_n^m(\theta) \equiv \tilde{W}_n^m(\theta) \Big/ \sqrt{n(n+1)} \tag{A20}$$

$$\overline{\Omega}_n^m(\theta) \equiv \tilde{\Omega}_n^m(\theta) \Big/ \sqrt{n(n+1)} \tag{A21}$$

The recursion coefficients for this normalization are:

$$\overline{a}_n^m = \begin{cases} \tilde{a}_n^m \sqrt{(n-1)/(n+1)}, & m > 0 \\ \tilde{a}_n^m, & m = 0 \end{cases} \tag{A22}$$

$$\overline{b}_n^m = \begin{cases} \tilde{b}_n^m \sqrt{(n-2)(n-1)/[n(n+1)]}, & m > 0 \\ \tilde{b}_n^m, & m = 0 \end{cases} \tag{A23}$$

$$\overline{c}_m = \tilde{c}_m \Big/ \sqrt{m(m+1)} \tag{A24}$$

$$\overline{d}_n^m = \tilde{d}_n^m \sqrt{(n-1)/(n+1)} \tag{A25}$$

$$\overline{e}_n = \tilde{e}_n \tag{A26}$$

The recursion relations are the same as equations (A6)–(A12) except that equations (A9) and (A12) respectively become:

$$\overline{P}_n^m = \overline{e}_n \sin\theta \, \overline{\Omega}_n^m \tag{A27}$$

$$\overline{V}_n^0 = -\overline{P}_n^1 \tag{A28}$$

[45] Fortran-90 code for computing $\tilde{P}_n^m$, $\tilde{V}_n^m$, and $\tilde{W}_n^m$ using this algorithm is provided in the auxiliary material. We validated the code, up to ($n$ = 72, $m$ = 72), against independent code that uses the Fourier method, which involves the solution of a tridiagonal system of equations [*Swarztrauber*, 1993]. With double-precision computation, the maximum difference between the output of the two codes was $2 \times 10^{-12}$, and our code was approximately three times faster. *Holmes and Featherstone* [2002] noted that the standard forward column method, applied at double precision, will produce numerical underflow for $m > 1900$; we therefore expect that our algorithm will produce reliable output for orders considerably higher than $m = 72$. However, as the order increases, our method will likely have less of an advantage in speed over the Fourier method.

[46] **Acknowledgments.** J. T. Emmert and D. P. Drob acknowledge support from the Office of Naval Research and from the NASA Living with a Star (LWS) Program (grant 04-000-0098). A. D. Richmond acknowledges support from the NASA LWS Strategic Capabilities Program and from AFOSR contract FA9550-08-C-0046. Geoff Crowley provided the TIME-GCM runs under NASA LWS grant 04-000-0098. IGRF parameters were obtained from http://www.ngdc.noaa.gov/IAGA/vmod/igrf.html.

[47] Robert Lysak thanks Vladimir Papitashvili and Stefan Maus for their assistance in evaluating this paper.

## References

Baker, K. B., and S. Wing (1989), A new magnetic coordinate system for conjugate studies at high latitudes, *J. Geophys. Res.*, *94*(A7), 9139–9143, doi:10.1029/JA094iA07p09139.

Crowley, G., T. J. Immel, C. L. Hackert, J. Craven, and R. G. Roble (2006), Effect of IMF $B_Y$ on thermospheric composition at high and middle latitudes: 1. Numerical experiments, *J. Geophys. Res.*, *111*, A10311, doi:10.1029/2005JA011371.

Drob, D. P., et al. (2008), An empirical model of the Earth's horizontal wind fields: HWM07, *J. Geophys. Res.*, *113*, A12304, doi:10.1029/2008JA013668.

Emmert, J. T., D. P. Drob, G. G. Shepherd, G. Hernandez, M. J. Jarvis, J. W. Meriwether, R. J. Niciejewski, D. P. Sipler, and C. A. Tepley (2008), DWM07 global empirical model of upper thermospheric storm-induced disturbance winds, *J. Geophys. Res.*, *113*, A11319, doi:10.1029/2008JA013541.

Fraser-Smith, A. C. (1987), Centered and eccentric geomagnetic dipoles and their poles, *Rev. Geophys.*, *25*, 1–16, doi:10.1029/RG025i001p00001.

Gustafsson, G., N. E. Papitashvili, and V. O. Papitashvili (1992), A revised corrected geomagnetic coordinate system for Epochs 1985 and 1990, *J. Atmos. Terr. Phys.*, *54*, 1609–1631, doi:10.1016/0021-9169(92)90167-J.

Hakura, Y. (1965), Tables and maps of geomagnetic coordinates corrected by the higher order spherical harmonic terms, *Rep. Ionos. Space Res. Jpn.*, *19*, 121–157.

Hein, C. A., and K. H. Bhavnani (1996), An expanded altitude algorithm for computing altitude-dependent corrected geomagnetic coordinates, *Rep. PL-TR-96-2274*, Phillips Lab., Hanscom Air Force Base, Barre, Mass.

Holmes, S. A., and W. E. Featherstone (2002), A unified approach to the Clenshaw summation and the recursive computation of very high degree and order normalised associated Legendre functions, *J. Geod.*, *76*, 279–299, doi:10.1007/s00190-002-0216-2.

Hultqvist, B. (1958a), The spherical harmonic development of the geomagnetic field, Epoch 1945, transformed into rectangular geomagnetic coordinate systems, *Arkiv Geophys.*, *3*, 53.

Hultqvist, B. (1958b), The geomagnetic field lines in higher approximation, *Arkiv Geophys.*, *3*, 63.

Killeen, T. L., R. G. Roble, and N. W. Spencer (1987), A computer model of global thermospheric winds and temperatures, *Adv. Space Res.*, *7*, 207–215, doi:10.1016/0273-1177(87)90094-9.

Mayaud, P. N. (1960), Un nouveau système de coordonnés magnétiques pour l'étude de la haute atmosphère: Les coordonnés de l'anneau équatorial, *Ann. Geophys.*, *16*, 278–288.

McIlwain, C. E. (1961), Coordinates for mapping the distribution of magnetically trapped particles, *J. Geophys. Res.*, *66*, 3681–3691, doi:10.1029/JZ066i011p03681.

National Imagery and Mapping Agency (NIMA) (2000), Department of defense world geodetic system 1984: Its definition and relationships with local geodetic systems, *Tech. Rep. TR8350.2*, Natl. Imagery and Mapp. Agency, Bethesda, Md. (Available at http://earth-info.nga.mil/GandG/publications/)

O'Brien, B. J., C. D. Laughlin, J. A. Van Allen, and L. A. Frank (1962), Measurements of the intensity and spectrum of electrons at 1000-Kilometer altitude and high latitudes, *J. Geophys. Res.*, *67*, 1209–1225, doi:10.1029/JZ067i004p01209.

Papitashvili, V. O., N. E. Papitashvili, G. Gustafsson, K. B. Baker, A. Rodger, and L. I. Gromova (1992), A comparison between two corrected geomagnetic coordinate systems at high-latitudes, *J. Geomagn. Geoelectr.*, *44*, 1215–1224.

Papitashvili, V. O., N. E. Papitashvili, and J. H. King (1997), Magnetospheric geomagnetic coordinates for space physics data presentation and visualization, *Adv. Space Res.*, *20*, 1097–1100, doi:10.1016/S0273-1177(97)00565-6.

Rangarajan, G. K. (1994), Secular variation in the geographic location of the dip equator, *Pure Appl. Geophys.*, *143*, 697–711, doi:10.1007/BF00879505.

Richmond, A. D. (1995), Ionospheric electrodynamics using Magnetic Apex Coordinates, *J. Geomagn. Geoelectr.*, *47*, 191–212.

Richmond, A. D., C. Lathuillére, and S. Vennerstroem (2003), Winds in the high-latitude lower thermosphere: Dependence on the interplanetary magnetic field, *J. Geophys. Res.*, *108*(A2), 1066, doi:10.1029/2002JA009493.

Roble, R. G., and E. C. Ridley (1994), A thermosphere-ionosphere-mesosphere-electrodynamics general circulation model (time-GCM): Equinox solar cycle minimum simulations (30–500 km), *Geophys. Res. Lett.*, *21*, 417–420, doi:10.1029/93GL03391.

Swarztrauber, P. N. (1993), The vector harmonic transform method for solving partial differential equations in spherical geometry, *Mon. Weather Rev.*, *121*, 3415–3437, doi:10.1175/1520-0493(1993)121<3415:TVHTMF>2.0.CO;2.

Vallado, D. A. (2001), *Fundamentals of Astrodynamics and Applications*, 958 pp., Microcosm Press, El Segundo, Calif.

VanZandt, T. E., W. L. Clark, and J. M. Warnock (1972), Magnetic Apex Coordinates: A magnetic coordinate system for the ionospheric $F_2$ layer, *J. Geophys. Res.*, *77*, 2406–2411, doi:10.1029/JA077i013p02406.

Yoshida, S., G. H. Ludwig, and J. A. Van Allen (1960), Distribution of trapped radiation in the geomagnetic field, *J. Geophys. Res.*, *65*, 807–813, doi:10.1029/JZ065i003p00807.

D. P. Drob and J. T. Emmert, Space Science Division, U.S. Naval Research Laboratory, Code 7643, 4555 Overlook Ave. SW, Washington, DC 20375, USA. (john.emmert@nrl.navy.mil)

A. D. Richmond, High Altitude Observatory, National Center for Atmospheric Research, PO Box 3000, Boulder, CO 80307, USA.